American Mineralogist, Volume 90, pages 252–257, 2005

LETTER

Pressure-induced stabilization of ordered paranatrolite: A new insight into the paranatrolite controversy

YONGJAE LEE,[1, 2,*] JOSEPH A. HRILJAC,[3] JOHN B. PARISE,[4] AND THOMAS VOGT[1,2]

[1]Physics Department, Brookhaven National Laboratory, Upton, New York 11973, U.S.A.
[2]Center for Functional Nanomaterials, Brookhaven National Labrotory, Upton, New York, 11973, U.S.A.
[3]School of Chemistry, University of Birmingham, Birmingham, B15 2TT, U.K.
[4]Geosciences Department, State University of New York, Stony Brook, New York 11794, U.S.A.

ABSTRACT

The origin and stability of paranatrolite (approximate formula $Na_{16-x}Ca_xAl_{16+x}Si_{24-x}O_{80}\cdot 24H_2O$), a naturally occurring zeolite with the natrolite topology, has long been debated, with its detailed structure unknown. When taken from an aqueous environment and exposed to the atmosphere, paranatrolite is reported to irreversibly lose water and transform to gonnardite/tetranatrolite, $Na_{16-x}Ca_xAl_{16+x}Si_{24-x}O_{80}\cdot nH_2O$. Since the latter has a disordered Al/Si distribution over the framework tetrahedral sites, it is believed the same is true for paranatrolite. Natrolite itself ($Na_{16}Al_{16}Si_{24}O_{80}\cdot 16H_2O$) has Al/Si ordering, and as recently shown, undergoes a reversible volume expansion (~2.5%) due to pressure-induced hydration (PIH) above 1.2 GPa to a superhydrated phase ($Na_{16}Al_{16}Si_{24}O_{80}\cdot 32H_2O$). During this process, an intermediate phase with an even *larger* volume expansion of ~7.0% has been detected in a narrow pressure range near 1.0 GPa. We report here that this intermediate phase has a unit-cell compatible with the one reported for paranatrolite at ambient conditions with the same 24 water molecules per formula unit and propose that it is paranatrolite with an ordered Al/Si distribution. An unusual water-sodium chain is observed in the ordered paranatrolite structure: a sevenfold coordination of sodium cations provided by alternating two water bridges along the expanded elliptical channels. The density of the ordered paranatrolite is *lower* than those of the 16 and 32 water phases, with its channel openings far more circular than in the low- and high-pressure analogs. The atomistic details of the ordered paranatrolite provide a structural model for the naturally occurring paranatrolite and a complete understanding of this intriguing pressure-volume-hydration mechanism in natrolite, demonstrating the unique role of pressure in controlling the chemistry of microporous materials.

INTRODUCTION

Zeolites are naturally occurring aluminosilicate minerals that adopt a variety of low-density framework structures made up of corner-connected (Al,SiO_4)-tetrahedra (Breck 1984). The framework contains windows that connect to pores and channels of molecular dimensions where charge-balancing cations and water molecules are located. The structure of the zeolite natrolite, $Na_{16}Al_{16}Si_{24}O_{80}\cdot 16H_2O$, was first proposed by Pauling and Taylor in the early 1930s (Pauling 1930; Taylor 1934). Its framework is composed of so-called fibrous chains of tetrahedra interconnected to generate elliptical channels along *c*-axis (Baur et al. 1990; Meier 1960). In the parent phase, silicon and aluminum atoms are ordered in framework tetrahedral (T) sites, and sodium cations and water molecules also adopt ordered arrangements along the channel. Chemical substitutions can occur both in the natrolite framework and charge-balancing cation sites, giving rise to a variety of analog mineral species such as scolecite, $Ca_8Al_{16}Si_{24}O_{80}\cdot 24H_2O$ (Kvick et al. 1985), mesolite, $Na_{5.3}Ca_{5.3}Al_{16}Si_{24}O_{80}\cdot 21.3H_2O$ (Artioli et al. 1986), gonnardite (Artioli and Galli 1999), and tetranatrolite (Evans et al. 2000). In scolecite and mesolite, the framework maintains an ordered Al/Si arrangement, but different degrees of Ca-exchange for Na leads to a monoclinic distortion or a tripling of the *b*-axis parameter of the parent orthorhombic natrolite unit cell, respectively. The composition and structural relationship of gonnardite and tetranatrolite is still controversial (Artioli and Galli 1999; Evans et al. 2000; Ross et al. 1992) but they have been reported to have a representative formulae of $Na_{16-x}Ca_xAl_{16+x}Si_{24-x}O_{80}\cdot nH_2O$ ($0.2 \le x \le 3.9$, $16 \le n \le 25.2$) and disordered Al/Si distributions at the framework T-sites. Paranatrolite is another natrolite analog with a high water content ($Na_{16-x}Ca_xAl_{16+x}Si_{24-x}O_{80}\cdot 24H_2O$ or ideally, $Na_{16}Al_{16}Si_{24}O_{80}\cdot 24H_2O$). It is claimed to transform irreversibly to tetranatrolite upon exposure to the atmosphere after removal from an aqueous environment (Chao 1980). It is therefore assumed that paranatrolite also has a disordered distribution of Al/Si over its framework T-sites (Chao 1980; Evans et al. 2000), and it is generally agreed that paranatrolite should not be considered as just a higher hydrate of natrolite (Evans et al. 2000). However, the only structural model for paranatrolite (Pechar 1988) has an ordered Al/Si distribution and was disputed by Baur (1991), who objected to the inappropriate conditions of the crystallographic measurement (no controlled humidity) as well as internal inconsistencies of the reported structural parameters. Belitsky et al. (1992) also observed that what they called natrolite II, which has unit-cell parameters similar to those of paranatrolite, forms reversibly from an ordered natrolite (natrolite I) at high water pressures. They speculated that natrolite II is an "overhydrated" analog of natrolite with a structure similar to that of paranatrolite (Belitsky et al. 1992). Subsequently, Paukov et al. (2002)

* E-mail: yollee@bnl.gov

proposed that Al/Si disordering has little effect on the thermodynamic properties of natrolite group zeolites.

We have recently demonstrated that the volume expansion of natrolite at pressures above 1.2 GPa occurs through the selective sorption of water molecules from the hydrostatic pressure transmitting fluid (Lee et al. 2002). This pressure-induced hydration (PIH) doubles the zeolitic water content from 16 to 32 H_2O molecules (per 80 framework O atoms), leading to a superhydrated phase and is reversible upon pressure release. During in situ X-ray diffraction studies of PIH, an intermediate phase with an even larger volume than the superhydrated phase but a lower water content of 24 H_2O molecules (per 80 framework O atoms), similar to the reported volume and water content of paranatrolite at ambient pressure, was detected as a mixed phase in a narrow pressure range between 0.8 and 1.2 GPa. Following this initial observation, subsequent experiments were successful in stabilizing a pure form of this intermediate phase. Here we present for the first time a detailed structural model of the intermediate phase at 0.99(10) GPa and discuss its relevance to the paranatrolite controversy.

Experimental details

Variable-pressure powder diffraction measurements were performed using a diamond-anvil cell (DAC) technique at beamline X7A of the National Synchrotron Light Source (NSLS). A powdered sample of natrolite (from Dutoitspan, South Africa, EPMA: $Na_{16}Al_{16}Si_{24}O_{80}\cdot 16H_2O$) was loaded into a 200 μm diameter sample chamber in a pre-indented stainless steel gasket, along with a few small ruby chips as a pressure gauge. A mixture of 16:3:1 by volume of methanol:ethanol:water was used as a pressure medium (hydrostatic up to ~10 GPa). The pressure at the sample was measured by detecting the shift in the *R*1 emission line of the included ruby chips. The sample pressure was gradually increased until 0.99(10) GPa where a pure monoclinic phase with ~7% volume expansion was obtained. No evidence of nonhydrostatic conditions or pressure anisotropy was detected during our experiments. The sample was equilibrated for about 30 min, and diffraction data were collected for 24 h with variable counting time [3–35° 2θ, λ = 0.6645(1) Å] using a micro-focused (~200 μm) monochromatic X-ray provided by an asymmetrically cut bent Si (111) monochromator and a gas-proportional position-sensitive detector (Smith 1991). The sample pressure was then raised to 1.77(10) GPa, and a pure superhydrated orthorhombic phase was observed. Three sets of diffraction data were measured during gradual pressure release; the pure monoclinic phase was observed again at 0.99(10) GPa, and appeared as a second phase on further release to 0.37(10) GPa. The fully released sample was a pure orthorhombic phase with a volume similar to that measured before the pressure cycle. The structure of the monoclinic phase at 0.99(10) GPa was refined using Rietveld methods and the GSAS suite of programs (Toby 2001) (see Tables 1–2).

Results and discussion

Changes of the unit-cell parameters and volume of natrolite as a function of hydrostatic pressures up to 5 GPa are shown in Figure 1. A volume increase of about 7.0% occurs at pressures near 1.0 GPa via expansions of the *a*- and *b*-axis parameters (4.0% and 4.2%, respectively) and a contraction of the *c*-axis parameter (1.2%). Further increase of pressure above 1.2 GPa results in the opposite behavior: the *a*- and *b*-axis parameters contract (2.5% and 2.2%, respectively) and the *c*-axis parameter expands (1.2%), leading to an overall volume reduction of 3.9% compared to that of the intermediate phase. The intermediate phase shows a monoclinic distortion of the original orthorhombic structure, as proposed for naturally occurring paranatrolite. Furthermore, the derived unit-cell parameters and volume are also close to those quoted for paranatrolite (Fig. 1) (Chao 1980). The structure of the phase above 1.2 GPa has been previously identified as the superhydrated state of natrolite with a doubled water content (Lee et al. 2002). When the pressure was gradually released from 1.7 GPa, the superhydrated natrolite material started to transform back to the intermediate phase at 1.1 GPa. However, further release of pressure below 0.8 GPa did not result

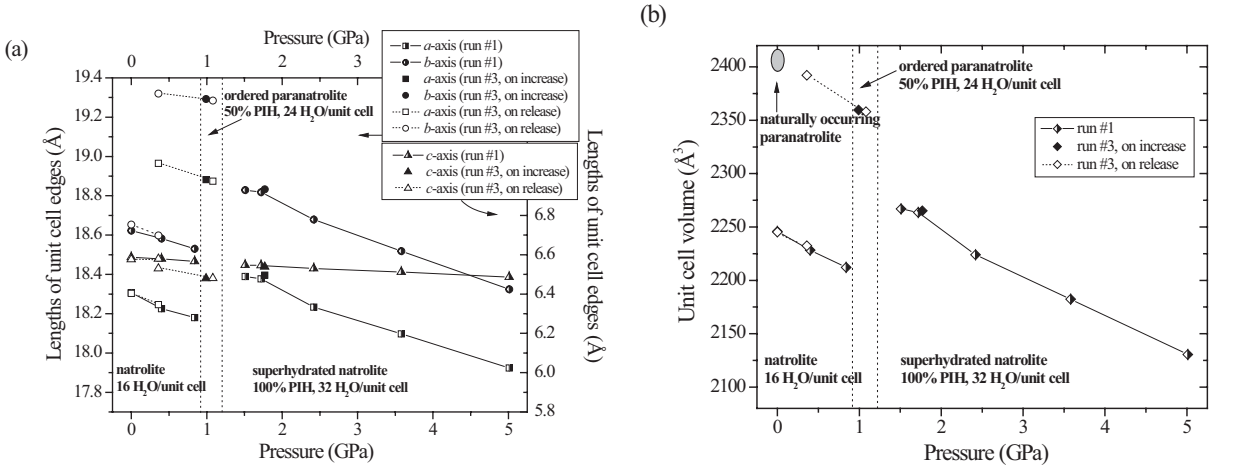

Figure 1. Pressure dependent evolution of (**a**) unit-cell edge lengths and (**b**) unit-cell volume, normalized to the orthorhombic setting with 80 framework O atoms, in natrolite ($Na_{16}Al_{16}Si_{24}O_{80}\cdot xH_2O$) under hydrostatic conditions mediated by an alcohol and water mixture. The filled symbols represent data taken on pressure increase and the unfilled symbols during pressure release. Data from Lee et al. (2002) were used to represent run 1 (half-filled symbols). For comparison, a grey ellipse is shown to represent the region of the reported volumes of naturally occurring paranatrolite at ambient pressure: a = 19.07(1), b = 19.13(1), c = 6.580(3) Å, V = 2400 Å^3 by Chao (1980); a = 19.02(1), b = 19.20(1), c = 6.606(4) Å, β = 91.56(4)°, V = 2412 Å^3 by Paukov (2002). Our ordered paranatrolite at 0.99(10) GPa has a = 18.882(1), b = 19.293(1), c = 6.4800(4) Å, β = 91.53(1)°, V = 2360(1) Å^3 (in pseudoorthorhombic setting, see supplemental table).[1]

[1]For a copy of this material, document item AM-05-004, contact the Business Office of the Mineralogical Society of America (see inside front cover of recent issue) for price information. Deposit items are available on the American Mineralogist web site at www.minsocam.org (or contact MSA Business Office for updated link information).

TABLE 1. Final refined atomic coordinates for the ordered paranatrolite at 0.99(10) GPa*

Atom	Site	*x*	*y*	*z*	Bond valence sum
Si1	4*a*	0.500	0.3746(11)	0.000	3.7
Si2	4*a*	0.195(5)	0.3322(11)	0.181(3)	3.7
Si3	4*a*	0.544(5)	0.0802(11)	0.314(3)	4.0
Al1	4*a*	0.936(5)	0.4645(11)	0.093(4)	2.7
Al2	4*a*	0.346(5)	0.2154(12)	0.402(4)	2.8
O1	4*a*	0.509(8)	0.0295(17)	0.436(4)	2.0
O2	4*a*	0.492(7)	0.0485(14)	0.159(4)	2.2
O3	4*a*	0.408(7)	0.1527(15)	0.293(4)	2.0
O4	4*a*	0.099(6)	0.1947(17)	0.442(5)	1.7
O5	4*a*	0.308(7)	0.2987(14)	0.336(4)	2.1
O6	4*a*	0.063(6)	0.2784(17)	0.059(4)	2.0
O7	4*a*	0.416(6)	0.3498(21)	0.134(3)	2.1
O8	4*a*	0.086(7)	0.4052(14)	0.224(4)	2.0
O9	4*a*	0.801(5)	0.1046(21)	0.355(3)	2.1
O10	4*a*	0.655(5)	0.4441(16)	0.040(5)	1.8
Na_{1A}	4*a*	0.180(7)	0.1587(17)	0.044(4)	1.0
Na_{1B}	4*a*	0.587(6)	0.0998(17)	–0.053(4)	1.3
OW_{2A}	4*a*	0.140(7)	0.0533(21)	–0.146(5)	
OW_{1A}	4*a*	0.932(9)	0.0743(24)	0.115(6)	
OW_{1B}	4*a*	0.368(8)	0.1905(25)	–0.098(5)	

Notes: In F*d* setting, $a = 18.882(1)$ Å, $b = 19.293(1)$ Å, $c = 6.4800(4)$ Å, $\beta = 91.53(1)°$, $x' = z/2$, $y' = y$, $z' = -x + z/2$. $_wR_p = 0.016$, $R_p = 0.014$, $\chi^2 = 2.7$. E.s.d. values are in parentheses. Soft constraints were used for framework interatomic distances. Restrained isotropic displacement parameters, U_{iso} (Å^2), were used for all atoms and refined to 0.013(1). All sites are fully occupied.
* Space group *Cc*, $a = 6.4800(4)$ Å, $b = 19.293(1)$ Å, $c = 9.8984(7)$ Å, $\beta = 107.56(1)°$.

TABLE 2. Selected interatomic distances (Å) and angles (°) for the ordered paranatrolite at 0.99(10) GPa*

Si1-O4	1.661(15)	Si2-O5	1.620(15)	Si3-O1	1.617(14)
Si1-O7	1.654(14)	Si2-O6	1.625(15)	Si3-O2	1.593(15)
Si1-O9	1.665(15)	Si2-O7	1.668(14)	Si3-O3	1.632(15)
Si1-O10	1.651(15)	Si2-O8	1.684(15)	Si3-O9	1.661(15)
avg.	1.658(7)†	avg.	1.649(7)†	avg.	1.626(7)†
Al1-O1	1.767(14)	Al2-O3	1.748(15)	Si3-O1-Al1	138.7(21)
Al1-O2	1.743(15)	Al2-O4	1.802(15)	Si3-O2-Al1	132.7(20)
Al1-O8	1.783(15)	Al2-O5	1.724(15)	Si3-O3-Al2	136.9(23)
Al1-O10	1.775(15)	Al2-O6	1.758(15)	Si1-O4-Al2	135.7(23)
ave.	1.767(7)†	ave.	1.758(8)†	Si2-O5-Al2	134.7(23)
Na_{1A}-O2	2.92(5)	Na_{1B}-O1	2.54(5)	Si2-O6-Al2	135.6(22)
Na_{1A}-O3	2.46(4)	Na_{1B}-O2	2.56(4)	Si1-O7-Si2	143.3(26)
Na_{1A}-O5	2.78(4)	Na_{1B}-O5	2.83(5)	Si2-O8-Al1	122.2(19)
Na_{1A}-O6	2.45(5)	Na_{1B}-O8	2.20(4)	Si1-O9-Si3	137.2(25)
Na_{1A}-OW_{2A}	2.73(5)	Na_{1B}-OW_{2A}	2.90(5)	Si1-O10-Al1	138.3(22)
Na_{1A}-OW_{1A}	2.53(5)	Na_{1B}-OW_{1A}	2.40(5)		
Na_{1A}-OW_{1B}	2.21(5)	Na_{1B}-OW_{1B}	2.21(6)		
OW_{2A}-O1	2.79(5)	OW_{1A}-O2	3.05(7)	OW_{1B}-O4	2.64(4)
OW_{2A}-O2	3.19(5)	OW_{1A}-O9	2.81(6)	OW_{1B}-O5	3.11(6)
OW_{2A}-O7	2.90(6)	OW_{1A}-O10	3.10(6)	OW_{1B}-O8	3.16(6)
OW_{2A}-O10	2.78(5)				
OW_{2A}-O10	3.15(5)				
OW_{2A}-OW_{1B}	3.00(5)				

* Estimated standard deviations are in parentheses.
† Standard deviations are computed using $\sigma = \frac{1}{n}\left(\sum_{i=1}^{n}\sigma_i^2\right)^{1/2}$.

in a complete transformation back to natrolite, and the data at 0.36(10) GPa on release showed a mixture of the intermediate phase and natrolite. Powder diffraction experiments of the recovered material confirmed that a complete pressure release to 1 bar and a subsequent loss of the pressure-transmitting fluid from the sample chamber led to the restoration of a pure natrolite sample. Unlike superhydrated natrolite, the intermediate phase exhibits a large hysterisis. Intriguingly, paranatrolite has been reported to occur in nature as epitactic intergrowths with natrolite crystals in aqueous environments (Chao 1980). This suggests that our intermediate phase may be stable (or metastable) at ambient pressure under such aqueous conditions (Chao 1980) or high relative humidity (Paukov et al. 2002), similar to those described for naturally occurring paranatrolite.

The structure of the intermediate phase was determined using monochromatic synchrotron X-ray powder diffraction data measured at 0.99(10) GPa and the Rietveld methods using a diamond-anvil pressure cell and Rietveld refinements (Rietveld 1969; Young 1995). The conventional space group *Cc* was used, and from difference Fourier maps an additional fully occupied water site was located along the natrolite channel. The derived unit-cell formulae, $Na_{16}Al_{16}Si_{24}O_{80}\cdot 24H_2O$, normalized to the orthorhombic setting, shows that the intermediate phase contains 8 more water molecules (24 water molecules per 80 framework O atoms) compared to the water content of natrolite at ambient conditions (16 water molecules per 80 framework O atoms). The calculated density of this intermediate phase at 0.99(10) GPa is 2.21 g/cm^3 (Fig. 2), the same as that reported by Chao (1980) for the naturally occurring paranatrolite (Chao 1980). It is interesting to note that the calculated density before PIH at 0.84(10) GPa is 2.26 g/cm^3, greater than that of the intermediate phase at 0.99(10) GPa. This indicates a less efficient packing of the water molecules and sodium cations inside the natrolite channel of the intermediate-pressure phase. As discussed earlier, a further increase in

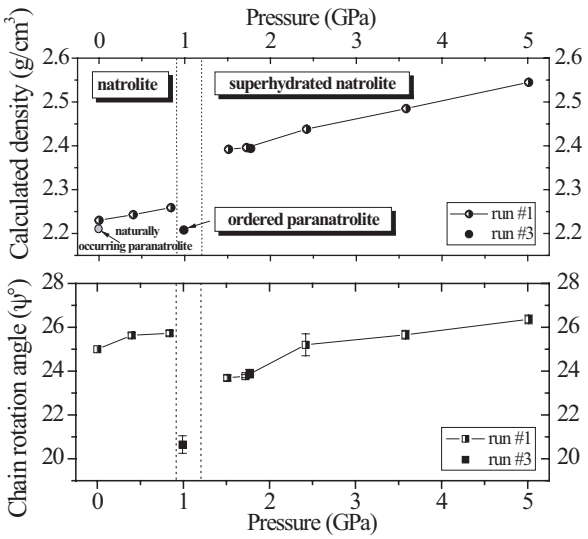

FIGURE 2. Pressure dependence of the calculated density (upper) and the overall rotation angle of the fibrous chains, ψ (lower). Measured density of naturally occurring paranatrolite at ambient pressure (2.21 g/cm^3 by Chao 1980) is shown as a grey circle for comparison. ψ is the mean of the angles between the sides of the quadrilateral around the T_5O_{10} (T = Al, Si) tetrahedral building unit projected on the plane along the natrolite channel (see Fig. 3). Data from Lee et al. (2002) were used to represent experiment no. 1 (half-filled symbols)

pressure above 1.2 GPa completes PIH and forms superhydrated natrolite, $Na_{16}Al_{16}Si_{24}O_{80}\cdot 32H_2O$, but results in a unit-cell volume reduction compared to the intermediate phase. This shows that the relative packing efficiency of the nonframework cations and water molecules now increases, with the calculated density of the superhydrated natrolite at 1.51(10) GPa increasing to 2.39 g/cm^3 from 2.21 g/cm^3. The observed volume expansion of the intermediate phase changes the elliptical channel opening into a

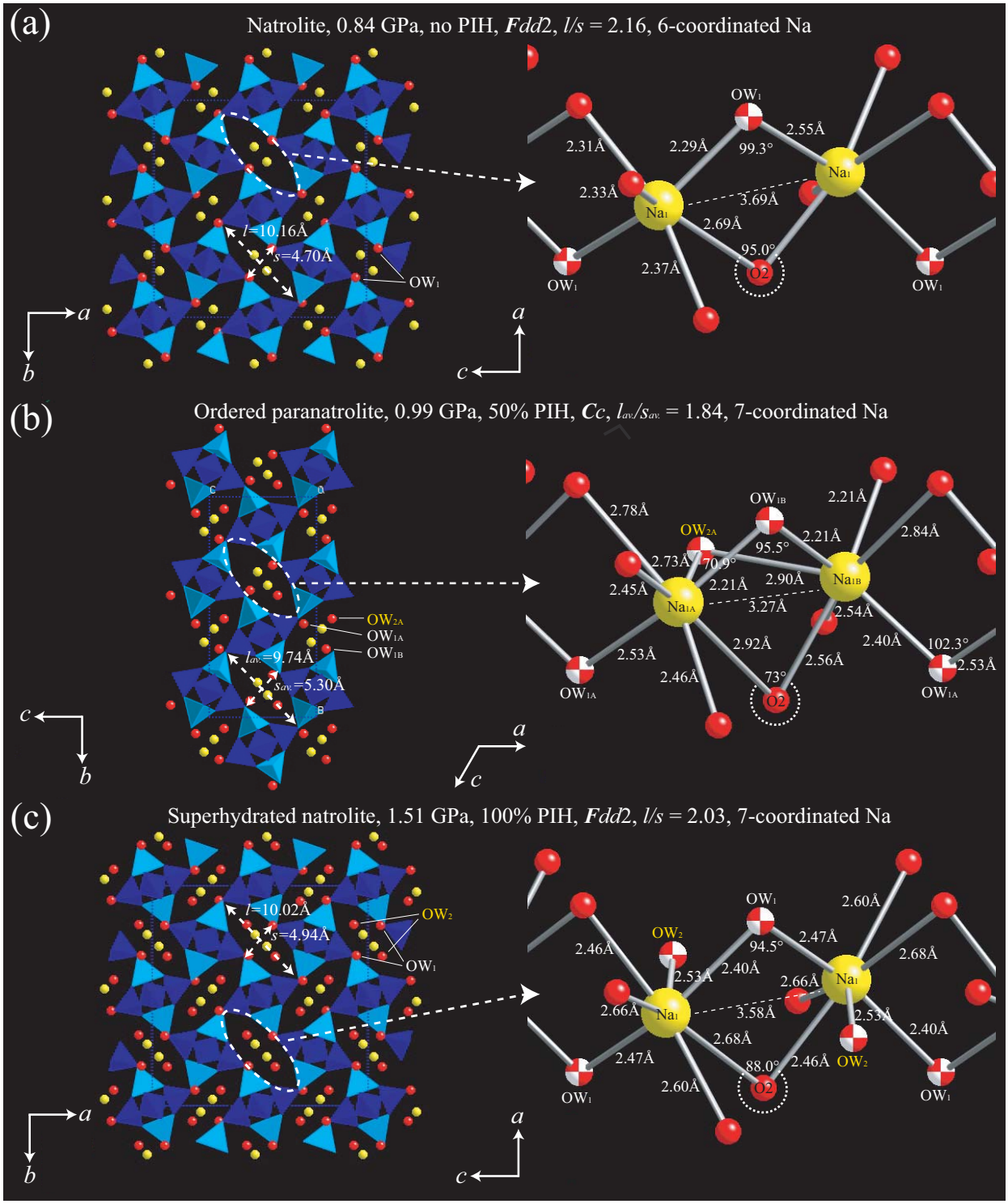

FIGURE 3. Polyhedral representations of natrolite ($Na_{16}Al_{16}Si_{24}O_{80}{\cdot}xH_2O$) with increasing level of pressure-induced hydration (PIH) viewed parallel to the channel (left) and expanded views of the nonframework sodium cations and water molecules viewed perpendicular to the channel (right). (**a**) Natrolite before PIH at 0.84(10) GPa, $x = 16$. (**b**) Ordered paranatrolite with 50% PIH at 0.99(10) GPa, $x = 24$. (**c**) Superhydrated natrolite with 100% PIH at 1.51(10) GPa, $x = 32$. Data from Lee et al. (2002) were used to represent the structures at 0.84(10) and 1.51(10) GPa. Tetrahedra are shown in two colors to illustrate the ordering of Al/Si over the framework tetrahedral sites. In figures to the right, yellow balls represent sodium cations, and O atoms from water molecules and the framework are shown as red/white balls and red balls, respectively. The ellipticity of the channel opening is illustrated by the ratio between long (l) and short (s) framework oxygen distances across the channel. Blue dotted lines in the figures to the left define unit cells, and white dotted lines in the right figures represent relaxation in Na-O2-Na angle and Na-Na separation distance during PIH.

more circular shape. A useful measure to estimate the degree of the natrolite framework collapse from its ideal geometry is the rotation angle of the fibrous chain, ψ, which is the mean of the angles between the sides of the quadrilateral around the T_5O_{10} (T = Al, Si) tetrahedral building unit projected on to the plane perpendicular to the channel (Baur et al. 1990). A greater value of ψ corresponds to a more elliptical channel. The ψ value of the intermediate phase is the smallest observed under pressure and clearly shows that its fibrous chains cover less pore space defined by the plane, hence the channel is less collapsed and more circular (Fig. 2).

The arrangements of the water molecules and sodium cations inside the channels of the intermediate phase reveal its distinct crystal-chemical features compared to those of natrolite and its superhydrated phase (Fig. 3). Regardless of the degree of PIH, the coordination number of the sodium cations increases from six (two water O atoms and four framework O atoms) to seven (three water O atoms and four framework O atoms). Unlike superhydrated natrolite, however, there are considerable rearrangements of the sodium cations into two symmetrically nonequivalent sites (Na_{1A} and Na_{1B}) in the channels of the intermediate phase. In natrolite before PIH at 0.84(10) GPa, two sodium cations in the symmetrically equivalent Na_1 site, separated by 3.69(2) Å, are bridged by a water molecule at the OW_1 site and a framework O atom at the O2 site which encloses an angle of 95.0(4)° with the two sodium cations (Fig. 3). In the intermediate phase, a newly inserted water molecule in the fully occupied OW_{2A} site along one edge of the elliptical channel provides an additional bridge and thereby shortens the Na-Na separation distance to 3.27(4) Å. As a result, a water-sodium chain with alternating double water bridges forms along the elliptical channel (Fig. 3). The average Na-O bond distance increases from 2.42(1) Å before PIH at 0.84(10) GPa to 2.58(2) Å (for Na_{1A}) and 2.52(2) Å (for Na_{1B}) in the intermediate phase at 0.99(10) GPa. Furthermore, in the intermediate phase the Na_{1A}-O2-Na_{1B} angle decreases dramatically to 73(1)°, thereby increasing the van der Waals envelope of the sodium-water chain perpendicular to the channel. This occurs in concert with the decrease of the chain rotation angle ψ leading to a more circular channel opening (Fig. 3). Upon full PIH at 1.51(10) GPa, the dispersion in the average Na-O bond distances then disappears and merges close to the mean value of 2.54(1) Å, thus making the sodium coordination environment less distorted than in the intermediate phase. At this stage, the additional water molecules, now located at the symmetrically equivalent OW_2 sites along both edges of the elliptical channels, bond to only one sodium cation instead of bridging two sodium cations, leading to a water-sodium chain with single water bridge, similar to that found in natrolite before PIH (Fig. 3). Concomitant with this, the Na_1-O2-Na_1 angle and the Na_1-Na_1 separation distance increase to 88.0(3)° and 3.58(2) Å, respectively. The chain rotation angle ψ increases up to 24°, thereby forming a slightly less elliptical channel opening than that in natrolite before PIH (Figs. 2 and 3).

The average Na-O bond distances correspond well to those observed for six- and seven-coordinated sodium (Baur and Khan 1970; Levy and Lisensky 1978; Wu and Brown 1975). This suggests that it is not energetically favorable to coordinate the new water molecule in the intermediate phase to only one sodium cation resulting in one sodium ion with sevenfold and the other with sixfold coordination. Instead, alternating double water bridging occurs and results in an increase in the coordination number of both sodium cations. This, in turn, leads to distortions of the sodium-oxygen (from both water molecule and framework) polyhedra and a subsequent expansion of the channel into a more circular shape. The extra pore space created in the intermediate state facilitates further hydration. In the superhydrated state, the channel reverts back to an elliptical shape and a single bridging mode is resumed.

Another important structural evolution during PIH can be found in the hydrogen bonding between water molecules. Before PIH, there is no hydrogen bonding between water molecules. In the intermediate phase, a new hydrogen bond forms between water molecules at the OW_{2A} and OW_{1B} sites with an O-O separation distance of 3.00(5) Å. This value is very close to that determined for a water dimer (Dyke et al. 1977; Odutola and Dyke 1980). Full PIH then leads to a formation of a network of 3-connected water molecules interpenetrating the natrolite channels and pores, with two short O-O distances of 2.80(4) Å and 3.09(4) Å, which can also be defined as a helical water nanotube along the natrolite channel (Lee et al. 2002). It has been shown that the rate of water diffusion in natrolite increases by a factor of ~10^4 near 0.8 GPa (Gabuda and Kozlova 1997; Moroz et al. 2001). We propose that the combination of the newly formed water dimers and the vacancies along one edge of the expanded natrolite channel in the intermediate phase is responsible for this unusual increase in water mobility.

In summary, we have unequivocally demonstrated that natrolite with an ordered Al/Si distribution transforms reversibly to an intermediate phase upon partial PIH. This intermediate phase is identified as an ordered form of paranatrolite, which is stable near 1.0 GPa. Given the anomalous increase in the channel opening and changes in the cation coordination environment, one may expect an increased ion exchange capacity in the ordered paranatrolite phase, which may be used as a host for "trap-door" ion exchange. The atomistic details of the phases of natrolite occurring during PIH reveal a fascinating and even counter-intuitive sequence, pointing to the rich high-pressure chemistry of microporous materials.

ACKNOWLEDGMENTS

This work was supported by an LDRD from BNL (Pressure in Nanopores). The authors thank G. Artioli for providing a specimen of natrolite. J. Hriljac acknowledges support from the Royal Society, and J. Parise acknowledges support from an NSF-DMR grant. Y. Lee acknowledges receipt of an Edward H. Kraus Crystallographic Research Grant from the Mineralogical Society of America. Research carried out in part at the NSLS at BNL is supported by the U.S. DOE (DE-AC02-98CH10886 for beamline X7A). We gratefully acknowledge the Geophysical Laboratory of the Carnegie Institution for access to their ruby laser system at beamline X17C.

REFERENCES CITED

Artioli, G. and Galli, E. (1999) Gonnardite: Re-examination of holotype material and discredition of tetranatrolite. American Mineralogist, 84, 1445–1450.

Artioli, G., Smith, J.V., and Pluth, J.J. (1986) X-ray structure refinement of mesolite. Acta Crystallographica, C42, 937–942.

Baur, W.H. (1991) Concerning the crystal-structure refinement of paranatrolite published by Pechar, F. Crystal Research and Technology, 26, 169–171.

Baur, W.H. and Khan, A.A. (1970) On the crystal structure of salt hydrates. VI. The crystal structures of disodium hydrogen orthoarsenate heptahydrate and disodium hydrogen orthophosphate heptahydrate. Acta Crystallographica, B26, 1584–1596.

Baur, W.H., Kassner, D., Kim, C.-H., and Sieber, N.H. (1990) Flexibility and distortion of the framework of natrolite: crystal structures of ion-exchanged natrolites. European Journal of Mineralogy, 2, 761–769.
Belitsky, I.A., Fursenko, B.A., Gubada, S.P., Kholdeev, O.V., and Seryotkin, Y.V. (1992) Structural transformations in natrolite and edingtonite. Physics and Chemistry of Minerals, 18, 497–505.
Breck, D.W. (1984) Zeolite Molecular Sieves. Krieger, Malabar, Florida.
Chao, G.Y. (1980) Paranatrolite, a new zeolite from mont St-Hilaire, Quebec. Canadian Mineralogist, 18, 85–88.
Dyke, T.R., Mack, K.M., and Muenter, J.S. (1977) Structure of water dimer from molecular-beam electric resonance spectroscopy. Journal of Chemical Physics, 66, 498–510.
Evans, H.T., Konnert, J.A., and Ross, M. (2000) The crystal structure of tetranatrolite from Mont Saint-Hilaire, Quebec, and its chemical and structural relationship to paranatrolite and gonnardite. American Mineralogist, 85, 1808–1815.
Gabuda, S.P. and Kozlova, S.G. (1997) Anomalous mobility of molecules, structure of the guest sublattice, and transformation of tetra- to paranatrolite. Journal of Structrual Chemistry, 38, 562–569.
Kvick, A., Stahl, K., and Smith, J.V. (1985) A neutron diffraction study of the bonding of zeolitic water in scolecite at 20K. Zeitschrift für Kristallographie, 171, 141–154.
Lee, Y., Vogt, T., Hriljac, J.A., Parise, J.B., and Artioli, G. (2002) Pressure-induced volume expansion of zeolites in the natrolite family. Journal of the American Chemical Society, 124, 5466–5475.
Levy, H.A. and Lisensky, G.C. (1978) Crystal structures of sodium sulfate decahydrate (Glauber's salt) and sodium tetraborate decahydrate (Borax). Redetermination by neutron diffraction. Acta Crystallographica, B34, 3502–3510.
Meier, W.M. (1960) The crystal structure of natrolite. Zeitschrift fur Kristallographie, 113, 430–444.
Moroz, N.K., Kholopov, E.V., Belitsky, I.A., and Fursenko, B.A. (2001) Pressure-enhanced molecular self-diffusion in microporous solids. Microporous Mesoporous Materials, 42, 113–119.
Odutola, J.A. and Dyke, T.R. (1980) Partially deuterated water dimers—microwave-spectra and structure. Journal of Chemical Physics, 72, 5062–5070.
Paukov, I.E., Moroz, N.K., Kovalevskaya, Y.A., and Belitsky, I.A. (2002) Low-temperature thermodynamic properties of disordered zeolites of the natrolite group. Physics and Chemistry of Minerals, 29, 300–306.
Pauling, L. (1930) The structure of some sodium and calcium aluminosilicates. Proceedings of the National Academy of Science, 16, 453–459.
Pechar, F. (1988) Structure refinement of paranatrolite by X-ray diffraction. Crystal Research and Technology, 23, 647–653.
Rietveld, H.M. (1969) A profile refinement method for nuclear and magnetic structures. Journal of Applied Crystallography, 2, 65–71.
Ross, M., Flohr, M.J.K., and Ross, D.R. (1992) Crystalline solution series and order-disorder within the natrolite mineral group. American Mineralogist, 77, 685–703.
Smith, G.C. (1991) X-ray imaging with gas proportional detectors. Synchrotron Radiation News, 4, 24–30.
Taylor, W.H. (1934) The nature and properties of aluminosilicate framework structures. Proceedings of the Royal Society, A145, 80–103.
Toby, B.H. (2001) EXPGUI, a graphical user interface for GSAS. Journal of Applied Crystallography, 34, 210–213.
Wu, K.-K. and Brown, I.D. (1975) A neutron diffraction study of $Na_2CO_3H_2O$. Acta Crystallographica, B31, 890–892.
Young, R.A. (1995) The Rietveld Method, 298 p. International Union of Crystallography, Oxford University Press, New York.

MANUSCRIPT RECEIVED DECEMBER 22, 2003
MANUSCRIPT ACCEPTED AUGUST 31, 2004
MANUSCRIPT HANDLED BY MARC HIRSCHMANN